Article ID: 1000-7032(2025)01-0012-11

WGM Lasing from Toroid-shaped ZnO Microdisk Pivoted on Si

ZHU Gangyi[1,2*], YAN Xinyue[2], YE Peng[2], QIN Feifei[2], WANG Zixuan[1], LI Binghui[3], LU Junfeng[4], WANG Xiaoxuan[5], XU Chunxiang[5]

(1. *College of Integrated Circuit Science and Engineering* (*College of Industry-Education Integration*), *Nanjing University of Posts and Telecommunications*, *Nanjing* 210003, *China*;

2. *GaN Optoelectronic Integration International Cooperation Joint Laboratory of Jiangsu Province*, *College of Telecommunications and Information Engineering*, *Nanjing University of Posts and Telecommunications*, *Nanjing* 210003, *China*;

3. *State Key Laboratory of Luminescence Science and Technology*, *Changchun Institute of Optics*, *Fine Mechanics and Physics*, *Chinese Academy of Sciences*, *Changchun* 130033, *China*;

4. *College of Physics*, *Nanjing University of Aeronautics and Astronautics*, *Nanjing* 211106, *China*;

5. *College of Electronic Science and Engineering*, *Southeast University*, *Nanjing* 210096, *China*)

* *Corresponding Author*, *E-mail*: *zhugangyi@njupt. edu. cn*

Abstract: Although it has a significant advantage in gain properties, the lack of selective etching processes hinders ZnO lasing in on-chip applications. Herein, the circular ZnO microdisk pivoted on Si substrate is fabricated through depositing ZnO on patterned silicon on an insulator (SOI) substrate. The cavity structure, morphology, and photoluminescence (PL) properties are studied systematically. The cavity shows a well-defined circular structure with oxygen vacancies. Under the synergistic action of surface tension and stress, the ZnO microdisk shows a unique toroid structure with a high sidewall surface finish. The ZnO microcavity (8 μm in diameter) shows optically pumped whispering gallery modes (WGMs) lasing in the ultraviolet region with a Q factor exceeding 1 300. More interestingly, the quality of the toroid ZnO microdisk cavity is high enough to support the bandgap renormalization (BGR) phenomenon. With the increasing pumping power, the lasing spectra will be modulated. The lasing spectrum undergoes a Burstein-Moss (BM) effect-induced blueshift and an electron-hole plasma (EHP) effect-induced redshift.

Key words: ZnO; microdisk; tunable lasing; molecular beam epitaxy

CLC number: TN248. 4　　**Document code**: A

DOI: 10. 37188/CJL. 20240242　　**CSTR**: 32170. 14. CJL. 20240242

硅基氧化锌微盘回音壁激光

朱刚毅[1,2*], 颜新悦[2], 叶　鹏[2], 秦飞飞[2], 王子轩[1], 李炳辉[3], 卢俊峰[4], 王潇璇[5], 徐春祥[5]

(1. 南京邮电大学 集成电路科学与工程学院(产教融合学院), 江苏 南京　210003;

2. 南京邮电大学 通信与信息工程学院, 江苏省氮化镓光电集成国际合作联合实验室, 江苏 南京　210003;

3. 特种发光科学与技术全国重点实验室, 中国科学院长春光学精密机械与物理研究所, 长春　130033;

收稿日期: 2024-09-30; **修订日期**: 2024-10-16

基金项目: 国家自然科学基金(62404040, 62204127); 江苏省自然科学基金(BK20215093); 江苏省双创博士项目资助基金(30644); 发光学及应用国家重点实验室(SKLA-2021-04); 省基础研究专项基金(自然科学基金)-面上项目(BK20241892, BK20221271); 智能纳米材料与器件教育部开放基金 NJ2020003(INMD-2021M11)

Supported by National Natural Science Foundation of China (62404040, 62204127); Natural Science Foundation of Jiangsu Province (BK20215093); the Foundation of Jiangsu Provincial Double-Innovation Doctor Program Grant (30644); State Key Laboratory of Luminescence and Applications (SKLA-2021-04); Provincial Basic Research Special Fund (Natural Science Foundation)-General Project (BK20241892, BK20221271); Open Fund of Key Laboratory for Intelligent Nano Materials and Devices of the Ministry of Education NJ2020003 (INMD-2021M11)

4. 南京航天航空大学 物理学院, 江苏 南京　211106;
5. 东南大学 电子科学与工程学院, 江苏 南京　210096)

摘要: 尽管ZnO激光器在增益特性方面具有显著优势,但ZnO材料的刻蚀工艺限制了任意大小尺寸微腔的制备,阻碍了它的片上应用。本文通过在绝缘硅(SOI)衬底上的图案化ZnO生长,制备了悬浮的ZnO微盘阵列,系统地研究了微腔的结构、形貌和光致发光(PL)特性。微腔具有圆形结构,在表面张力和应力的协同作用下,ZnO微盘呈现出独特的环形结构,并且侧壁表面光滑。ZnO微盘(直径8 μm)获得的光泵浦回音壁模(WGMs)紫外激光,Q因子超过1 300。更有趣的是,由于微腔对光与物质相互作用的增强,ZnO微盘腔的光学品质良好,支持了ZnO材料在高激发态下的带隙重整化(BGR)现象,激光模式也随着一起被调制。实验结果表明,随着泵浦功率的增加,激光光谱经历了Burstein-Moss(BM)效应引起的蓝移和电子空穴等离子体(EHP)效应引起的红移。

关　键　词: 氧化锌; 微盘; 可调谐激光; 分子束外延

1　Introduction

The on-chip integration of micron and sub-micron laser sources with high gain and cavity quality is significant for emerging photonic applications[1-2]. However, three issues behind it will highly influence the performance of micron and sub-micron lasers. The previous research results indicate that these influence factors are materials quality, fabrication technology, and optical loss caused by optical coupling to the substrate or rough sidewalls[3-4]. Zinc oxide(ZnO), a competent material with intrinsic direct wide bandgap (up to 3.37 eV), large exciton binding energy (~60 meV), and low bio-toxicity[5-7], has attracted considerable interest for short-wavelength laser applications. Since the early observation of lasing from ZnO film by D. M. Bagnall in 1997[8], remarkable attempts have been made to realize high-quality lasers from ZnO nanowires, micro-rods, nanobelts, and spheres[9-12]. However, due to the amphoteric oxide properties, typical microfabrication methods such as lithography, reactive ion etching (RIE), or inductively coupled plasma (ICP) are unsuitable for the etching of ZnO. Hence, most reported lasing is realized in a natural microcavity, which hinders the further demonstration of suspended photonic devices based on ZnO crystals.

Circularly shaped microdisks with smooth surface finish are superior to most other dielectric microresonator structures to support whispering gallery mode (WGMs) lasing. It allows light to be trapped on much longer timescales, resulting in higher quality (Q) factors, lower lasing thresholds, and less demand for gain material[13-14]. Combining the high gain of ZnO and circular cavity structures may be a practical approach to getting a high-performance laser. However, strategies are needed to realize circular ZnO microdisk and integrate it onto a silicon substrate. Interestingly, Liu *et al.* once proposed the fabrication of ZnO microdisks on pre-patterned silicon substrates by the metal-organic chemical vapor deposition (MOCVD) method[15]. Although different lattice constants and thermal expansion coefficients exist between Si and ZnO, this is still a vital attempt to realize suspended ZnO microdisk lasing on a Si substrate[16].

In this paper, we fabricate circular ZnO microdisks on a Si substrate *via* molecular beam epitaxy (MBE) growth of ZnO on patterned silicon on an insulator (SOI) substrate which can "co-integrate" compound semiconductors[17]. Compared with other methods, the SOI substrate can help us get high-quality ZnO with a controllable toroid structure. The ZnO microdisk's structural, defect, and optically pumped lasing properties are studied. The samples are well crystalline. Under the synergistic action of surface tension and stress, the ZnO microdisk shows a unique toroid structure with a high sidewall surface finish and low optical loss. Whispering gallery mode (WGM) lasing is realized, and bandgap renormalization (BGR) induced lasing mode tuning is further observed. The lasing spectrum first undergoes a blueshift, followed by a redshift with increased pumping power. Our work may benefit the development of a high-quality, wavelength-tunable laser on a chip scale and need much effort to be developed[18].

2 Experiment

2.1 Fabrication of Toroid-shaped ZnO microdisk

The pivoted ZnO microdisk is fabricated using a standard micro-fabrication process by two-step methods. In the first step, a suspended Si microdisk pattern is made *via* the lithography (Fig. 1(a)-(b)), ICP etching (Fig. 1 (b)-(c)), and BOE solution isotropic wet etching of SOI substrate (Fig. 1(d)-(e))[19]. The ZnO layer is epitaxially grown on the patterned substrate using MBE methods in the second step[20]. The patterned SOI substrate is exceeding preheated in the oven for 2 h under 750 ℃. The ZnO layer is grown onto the substrate at a Zn source temperature of 370 ℃, substrate temperature of 600 ℃, oxygen flow of 1.26–1.43 mL/min, and pressure of 8×10^{-4} Pa. Diameter of the disk can be controlled by the pattern size. During the MBE process, the Si disk will gradually be transformed to SiO_2 under oxygen-rich and high-temperature conditions. The synergistic effect of strain and surface tension of multi-layer materials highly influences the shape of the cavity. Lattice mismatch-induced strain between ZnO and Si will roll up the device. Similar to D. K. Armani's research[21], melting of the SiO_2 substrate occurs along the periphery. It is vital to have a good cavity structure and a smooth surface to reduce optical losses and improve light field confined abilities[22]. In this case, the surface tension will be produced, and it will help to smooth the surface and collapse the ZnO disk to a toroid shape with limiting dimensions defined by the support pillar and the initial thickness of the SiO_2 layer[23]. Finally, a circular ZnO microdisk with a toroid shape can be obtained (Fig. 1(g)).

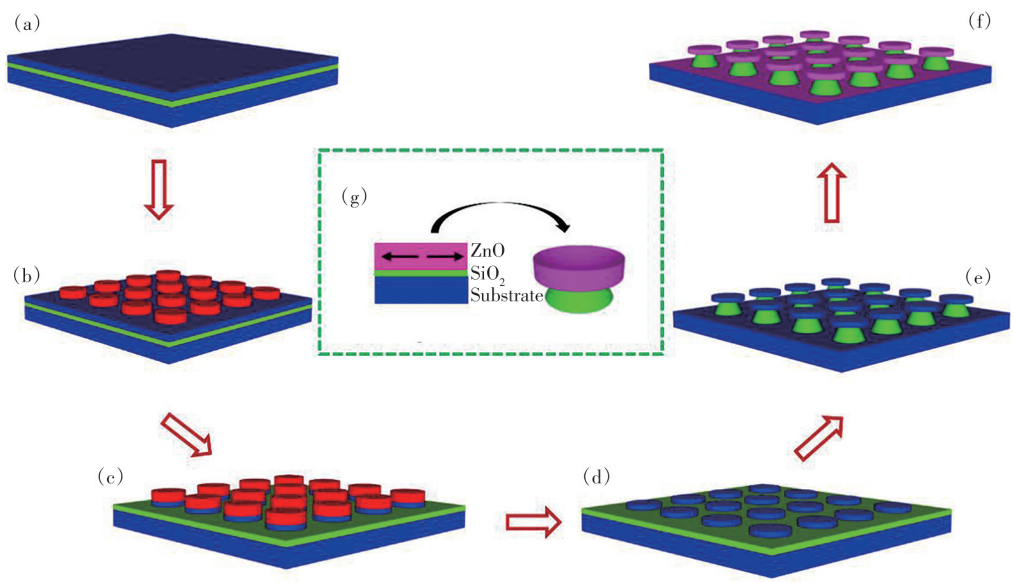

Fig.1 Fabrication process of ZnO microdisk suspended on Si substrate. (a) Primary SOI substrate. (b) Patterned Si microdisk. (c) ICP etching of Si microdisk. (d) Removing of photoresist. (e) Wet etching of SiO_2 middle layer. (f) Growth of ZnO microdisk *via* MEB process. (g) Mechanism of a toroid of device

2.2 Sample Characterization Methods

Scanning electron microscopy (SEM; Hitachi SU-8010) and atomic force microscope (AFM; NTEGRA Spectra C) characterize the samples[24]. The X-ray diffraction pattern is recorded with an X-ray diffraction instrument (XRD; Brooker D8 advance). X-ray photoelectron spectroscopy (XPS; Shimadzu AXIS) is used to confirm the lattice defects of ZnO. A confocal micro photoluminescence (μ-PL) setup (Olympus BX35) excited by a 325 nm nano-second pulsed laser is used to measure samples' PL and lasing spectra. A spectrometer (Princeton *et al*. SP2500i) resolves the PL's spectra. TRPL spectra are measured with the same setup, and the signal is recorded with a streak camera system (Optronics GmbH SC-10).

2.3 FDTD Simulation Method

Lasing resonant of cavities is simulated using the 2D-FDTD method[25-26]. During this process, a dipole light source with a similar wavelength region of PL (350–420 nm) is used. To simplify the process, a ZnO microdisk with different diameters is used as the simulation mode. The frequency domain field is set to record the electrical field distribution with resonant wavelength.

3 Results and Discussion

SEM of individual Si microdisk is shown in Fig. 2(a). It is smooth, thin, and pivoted with a middle Si pillar with a thickness of 220 nm. Since the SiO_2 layer is etched away, the sample will be suspended by about 2 μm. With the patterned substrate consisting of a Si microdisk array, circular ZnO microdisks with diameters of 4 μm, 8 μm, and 13 μm are fabricated (Fig. 2(b)–(d)). A ZnO layer with a thickness of approximately 0.9 μm to 1 μm is attached to the substrate. The cavity is suspended up to the Si with a gap of about 2 μm which can improve the optical properties effectively[27]. The AFM result in Fig. S1 indicates that a small particle appears on the surface, and the RMS roughness is in the 8–12 nm region. Many small grains are visible in the cross-section SEM of the microdisk with 4 μm and 13 μm. The strain and surface tension in multilayers during the sample fabrication process make the 8 μm ZnO microdisk show a relatively smooth sidewall. Interestingly, the outer ring of the ZnO microdisk rolls up slightly with a toroid structure. It is advantageous for enhancing the light field in the vertical direction. Moreover, a microdisk array can also be obtained (Fig. 2(i)) with a well-designed SOI substrate. EDX mapping of individual ZnO microdisks in Fig. 2(e)–(g) confirms that the Zn, Si, and O elements are distributed uniformly and distinctly, corresponding to the surface of the ZnO microdisk. The Si signal in Fig. 2(e) is more robust, and there is a clear boundary between substrate and microdisk.

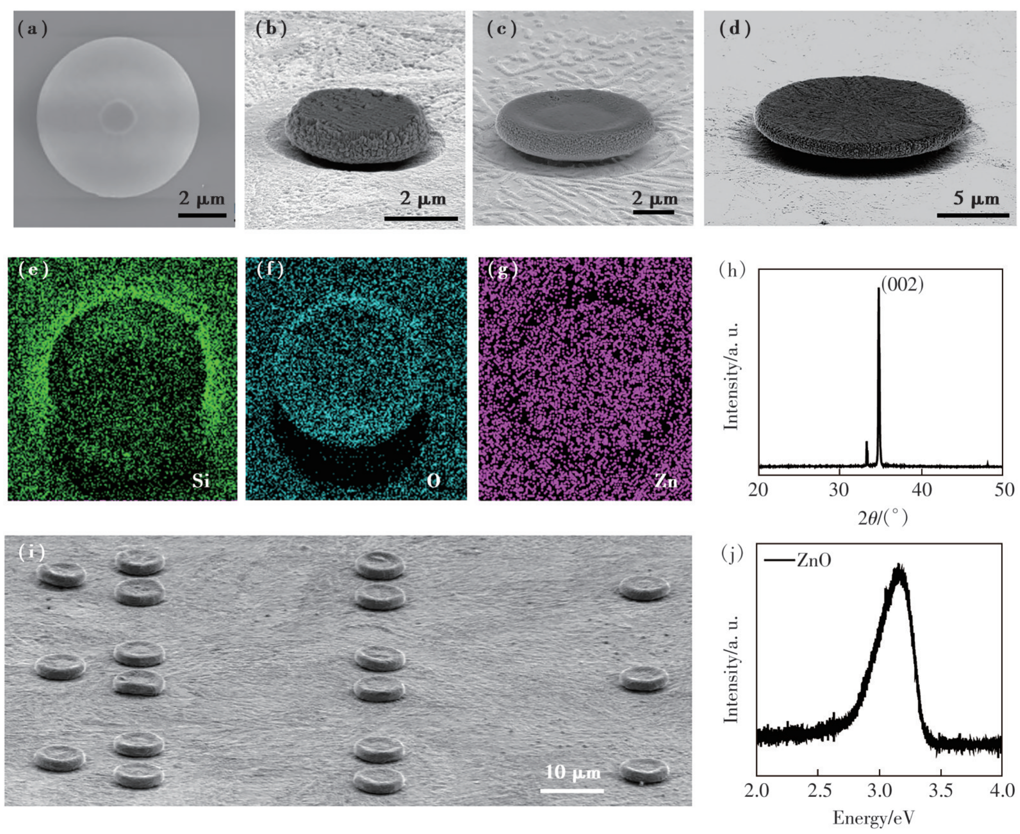

Fig.2 SEM images of single Si microdisk(a), ZnO microdisk with a diameter of 4 μm, 8 μm, 13 μm((b)–(d)), and 8 μm ZnO microdisk array(i). EDX mapping((e)–(g)), XRD pattern(h), and normalized PL spectra(j) of epitaxial grown ZnO cavity

XRD and XPS measurements characterize the material quality and surface condition of ZnO. A typical XRD pattern of the floating ZnO microdisk is shown in Fig. 2(h). It is a polycrystal film with two diffraction peaks appearing in the region of 20°−50°. The high intensity of the (002) diffraction peak reveals the growth direction of [0001], which fits the wurtzite phase of ZnO (JCPDS No. 36-1451)[28]. Due to the high gain properties of ZnO, although the sample is not smooth, it still can hold lasing oscillation. Fig. 2(j) shows the normalized PL spectrum of the ZnO film. The UV emission with band energy near 3. 18 eV is due to the direct recombination of excitons or surface impurities[29-30]. XPS results in Fig. 3 further confirm the lattice defects of the MBE sample. A broad survey scan of XPS spectra in the 0–1 200 eV region is taken and shown in Fig. 3(a).

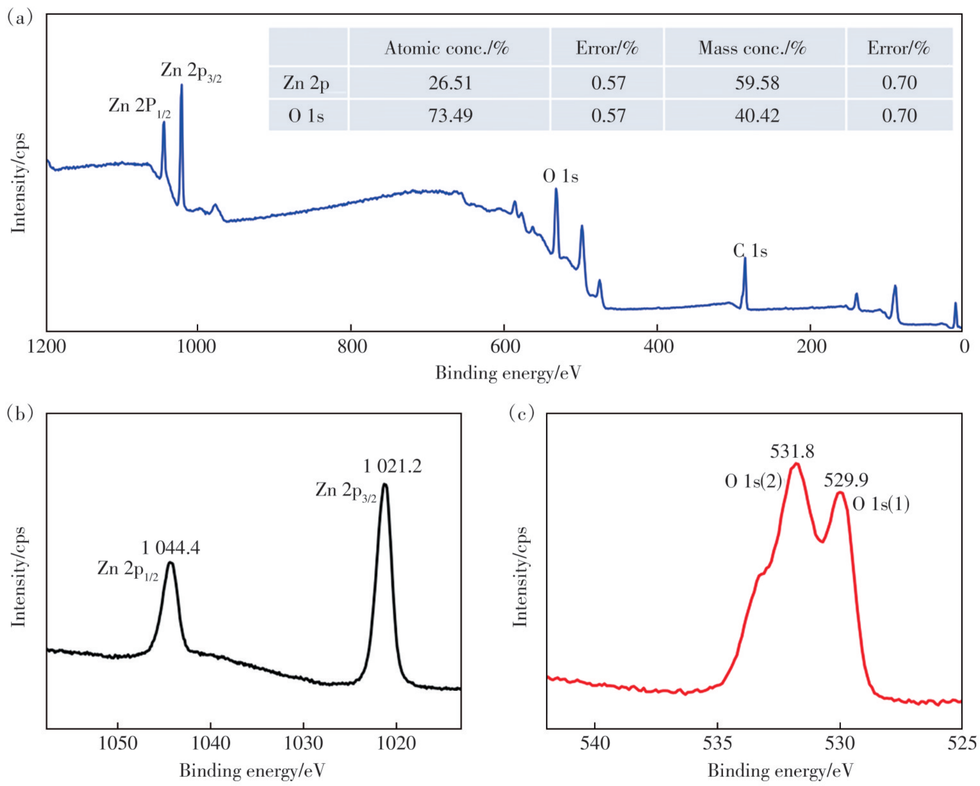

Fig.3 (a)Wide survey X-ray photoelectron spectrum of epitaxially grown ZnO cavity. Zn 2p spectrum(b) and O 1s spectrum(c) of ZnO. The inset table shows the atomic ratio and mass rate of Zn and O

Typically, an internal reference peak (C 1s) at a binding energy of 284. 6 eV appears[31]. Peaks corresponding to Zn 2p and O 1s are also observed. The ratios of Zn and O are 26. 51% and 73. 49% in atomic concentrate and 59. 58% and 40. 42% in mass concentrate. As shown, the O content is much higher than that of Zn. Considering the high-temperature and oxygen-enrichment conditions during the growth of ZnO, the Si substrate is oxidized to SiO_2. Thus, the excess oxygen element may come from the SiO_2. Fig. 3(b), (c) show the XPS details of Zn 2p and O 1s. The Zn 2p spectrum shows a doublet with 1 021. 2 eV (Zn $2p_{3/2}$) binding energies and 1 044. 4 eV(Zn $2p_{1/2}$). The binding energy difference between the two lines is 23. 2 eV, which lies well within the standard reference value of ZnO. The lower binding energy component of O 1s at 529. 9 eV is attributed to the wurtzite structure of hexagonal Zn^{2+} ion, and the higher binding energy component at 531. 8 eV is attributed to the oxygen-deficient region ZnO. In comparison, the shoulder at 533. 7 eV is attributed to OH- groups at the ZnO surface[32].

The high-evolution PL and exciton recombination properties of individual 8 μm samples are studied in detail. As shown in Fig. 4(a), a transformation from spontaneous to stimulated emission is obtained for a pumping power of 0. 6–6. 6 μW. The resonant mode with a peak wavelength near 400. 71 nm appears with a threshold value of 5. 6 μW in Fig. 4(b). It changes to 402. 10 nm for a higher excitation power. The lasing mode is stable at various pumping powers. The characteristic resonant spectra are shown in Fig. 4(c). For pumping power below threshold values, the spectra belongs to the spontaneous radiation. And the lasing oscillation appears for the pumping power above threshold values, and the resonant peaks lie at 397. 76 nm, 400. 22 nm, 402. 17 nm and 404. 22 nm. Considering ZnO's size and cavity structure in Fig. 2(i), a possible resonant mechanism is the WGM based on the inner wall's total reflection. Power-dependent lasing spectra of samples with other diameters are shown in Fig. S2. Similar spontaneous and stimulated emission appears for each sample. Comparing with the results in Fig. 4(a) and Fig. S2, we can see that the sample with a diameter of 8 μm has the most special lasing properties. It has a lower full width at half maximum (FWHM) and a higher *Q* factor, but the threshold value increases with the addition of diameter (see details in Tab. S1).

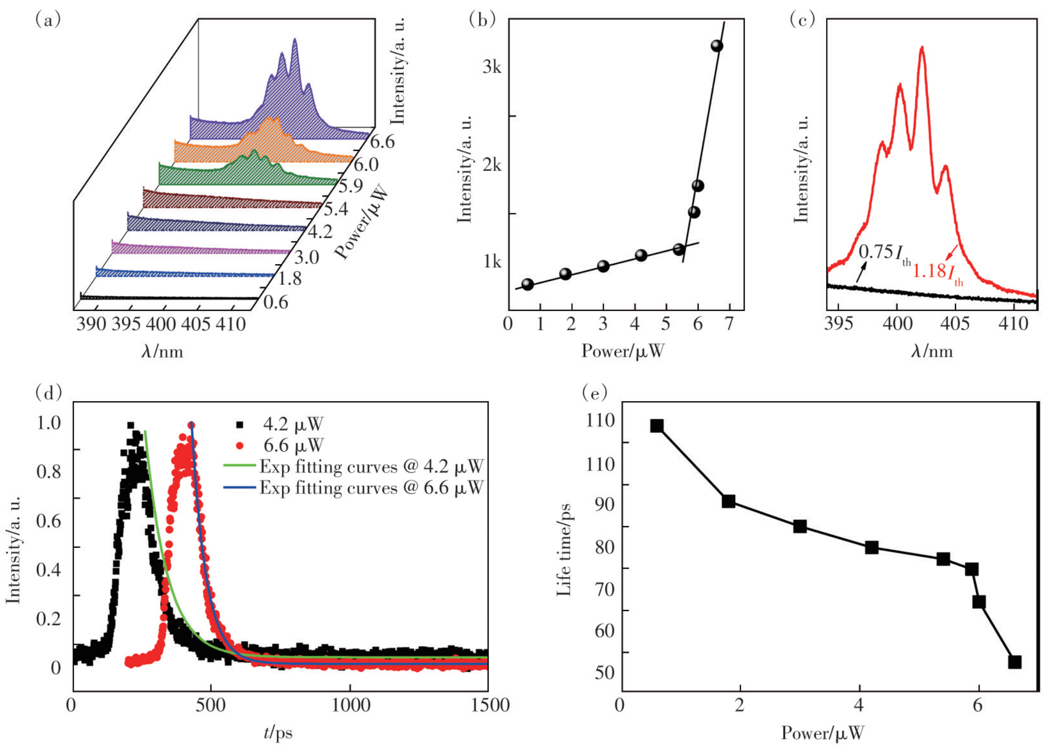

Fig.4　Optical pumped lasing properties (a), threshold curves (b), and the characteristic spectrum (c) of a ZnO microdisk (8 μm). (d) Normalized TRPL spectra with a central wavelength and its fitting curves. (e) Power dependent carrier combination time summary of peak wavelength

The time-resolved PL (TRPL) extraction spectra are used to evaluate the crystal quality, which becomes longer as the quality improves. Together with the lasing spectra in Fig. 4(a), carrier combination properties of the ZnO microdisk were recorded. The TRPL spectra with a single exponential fitting of a ZnO microdisk (8 μm) at room temperature are shown in Fig. 4(d)–(e). The PL intensity decays by approximately 80 ps for spontaneous emission at power of about 4. 2 μW (below threshold values), shorter than single-crystal ZnO[33]. However, this value is in the region of poor crystal quality (~30 ps) to a high crystal quality of ZnO (~110 ps) grown *via* the MBE method[34]. The stimulated emission at 6. 6 μW (above threshold value) is faster than the spontaneous emission with an exciton combination time. The lifetime decreases with increasing pumping power in Fig. 4(e).

To further study the structural-related light emission properties, typical lasing spectra of the as-grown samples with a diameter of 4 μm, 8 μm and 13 μm are measured and shown in Fig. 5(a). Stimulated emission appears for each cavity in the gain region of 385 nm to 395 nm. As mentioned before, considering cavity size in Fig. 2(b)-(d) and the lasing spectra in Fig. 5(a), most of the mechanism is WGM resonant in the circular microdisk. Eq. (1)-(3) provide the calculation equation for Q factor, resonant mode number(N), and free spectral range(R) of WGM lasing with peak wavelength λ, FWHM, $\Delta\lambda$, cavity diameter D, refractive index n, and dispersion relation $dn/d\lambda$[35-37]:

$$Q = \lambda/\Delta\lambda, \quad (1)$$

$$N = n\pi D/\lambda, \quad (2)$$

$$R = \lambda^2/\pi D(n - \lambda dn/d\lambda). \quad (3)$$

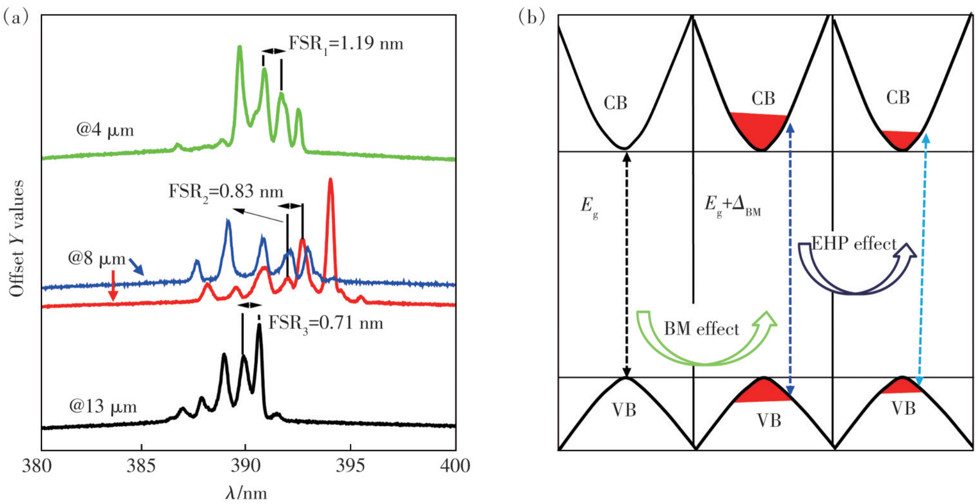

Fig.5 (a)Cavity size dependent lasing resonant of circular ZnO microdisk. (b)An illustration of the various effects on the band gap energy of ZnO: primary band gap, filled band gap, relaxed band gap

Based on Eq. (1) and the spectra in Fig. 5(a), the calculated Q factor is 1 217 (with λ as 389.5 nm, $\Delta\lambda$ as 0.32 nm) and 1 301 (with λ as 390.4 nm, $\Delta\lambda$ as 0.30 nm) for microdisks with 4 μm and 13 μm diameter, respectively, and the Q value for 8 μm samples can reach 1 354 (with λ as 393.9 nm, $\Delta\lambda$ as 0.291 nm). The high Q factor confirms the high cavity quality of 8 μm samples. As shown in Fig. 2(a)-(d), many sub-micro grains on the edge of the disk appear, leading to increased light leakage, thus affecting the reduction in the Q factor. The 8 μm sample's surface is smooth, and it has the highest Q factor. According to Eq. (2) and Eq. (3), the mode number increases with the increased cavity size, and the FSR decreases with the increase of cavity size and resonant wavelength. These results are consistent with the results in the electromagnetic field distribution of Fig. S3 in supporting documentation, and the sample with 8 μm in diameter can limit the light in the cavity well with explicit resonant modes.

Due to the exemplary cavity quality and applicable exaction combination properties in Fig. 4(e), the most likely reason for power-dependent spectra modulation of 8 μm samples is bandgap renormalization (BGR)[38]. In this case, under photon excitation, the valence band electrons transition move to the conduction band, and the electron density n_e of ZnO can be estimated by $n_e = \beta \cdot I_{exc}/hw_{exc}$ with absorption coefficient ($\beta = 1.6\times10^5$ cm^{-1})[39-40]. As demonstrated in Fig. 5(b), with the increased pumping power, if n_e reaches the 10^{19} cm^{-3} level[41-42], Burstein-Moss (BM) effect[43-45] featured with increased bandgap will happen. If further increasing the electron density n_e to the Mott density of ZnO (3.7×10^{19} cm^{-3})[46], the electron-hole plasma(EHP) effect featured with decreased bandgap will appear.

To further demonstrate the bandgap renormalization-induced lasing properties, the power-dependent lasing properties of an optimized microdisk (8 μm) are studied in detail. In the experiment, a 325 nm laser with a repetition rate of 1 000 Hz, a pulse width of 150 fs, and a spot diameter of 30 μm is used as the light source. The calculated electron density n_e for pumping power in μW level is high enough to support the BM and EHP phenomena in high-quality ZnO microcavities. Similar to Fig. 4(a), broad spontaneous emission is observed at a low pump power of 5.7 μW (Fig. 6(a)). Lasing resonance with a peak wavelength of 401.2 nm and Q factor of 1 215 appears for a pumping power of 5.9 μW. A blueshift occurs in the spectrum for pumping power above 6.7 μW, and the spectrum demonstrates a red shift when pumping power is increased to 9.1 μW. The lasing oscillation's first blue and then red shift can be attributed to the bandgap renormalization. In this case, the gain properties of the sample will be changed. And it will further influence the lasing properties of Fig. 6. This process can be re-demonstrated by decreasing the pumping power. As shown in Fig. 6(b), the lasing spectra are first blueshifted and then redshifted for pumping power decreasing from 15.6 μW to 4.8 μW. To further understand the lasing parameters, based on the data in Fig. 6, the power dependent peak intensity, FWHM and FSR are summarized and shown in Fig. S4. With the increasing of pumping power, the peak intensity is improving and then decreased with the fall up of pumping power. However, the FWHM and FSR fluctuate with the pumping power. FWHM is in the same level of values in Tab. S1. FSR fluctuates in the region of 0.63 nm to 1.61 nm.

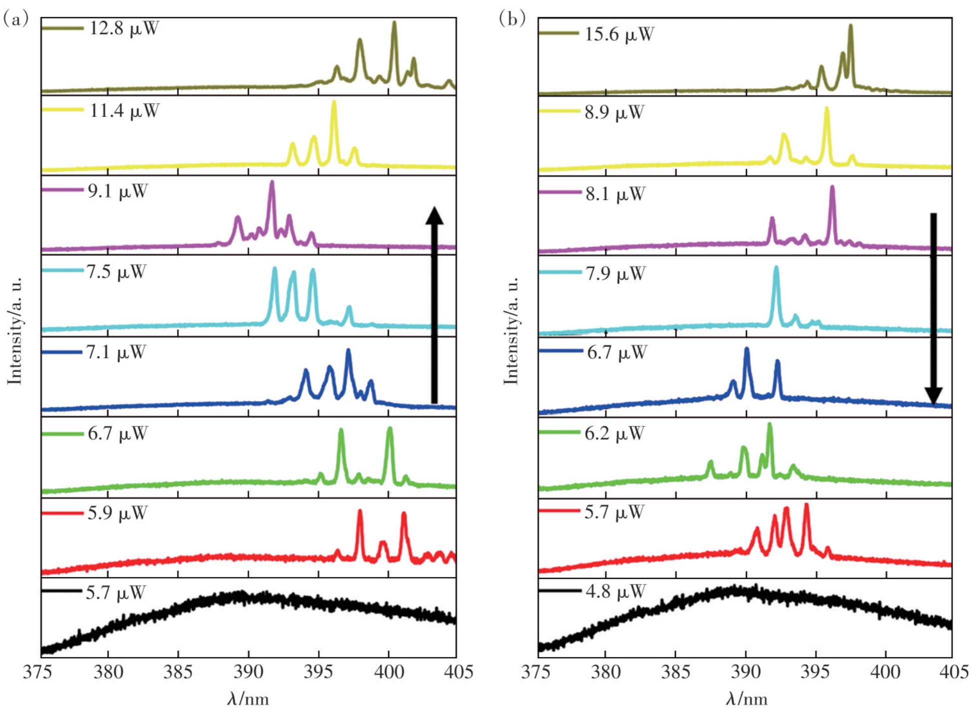

Fig.6 Power-dependent lasing spectra of ZnO microdisk of diameter 8 μm: (a) from low power to higher power, (b) from high power to low power

4 Conclusion

In summary, with the patterned SOI substrate and MBE methods, a toroid-shaped ZnO microdisk pivoted on Si is fabricated using a standardized process. Samples with a diameter of 4 μm, 8 μm, and 13 μm can be obtained *via* a well-designed pattern. XRD and XPS analysis indicate that the samples show a well-hexagonal wurtzite structure with temporary oxygen vacancy. Lattice mismatch-induced strain and melting-induced surface tension in the multi-layer exist during the sample fabrication. Finally, the ZnO microdisk is slightly rolled up with a shaped structure. The circular and toroid cavity structure ensures the well-light confirm effect. Thus, the energy density of the cavity is high, and the optical loss of the cavity is low. Under optical pumping, carrier combination time reaches 80 ps, and lasing resonance appears in cavities with varying diameters. The toroid cavity structure of the 8 μm sample shows a high *Q* factor of over 1 300, and it can support pumping power-induced bandgap renormalization. With the increased pumping power, the lasing spectra demonstrate blue and red shifts, which can be attributed to the BM and EHP effects. Our study provides a new growth fabrication method for obtaining a circular ZnO microdisk integrated into a silicon substrate, which may benefit the realization of future chip-based optoelectronic circuitry.

Supplementary Information and Response Letter are available for this paper at: https://cjl.lightpublishing.cn/zh/article/doi/10.37188/CJL.20240242/

References:

[1] HANSEN R P, ZONG Y Q, AGRAWAL A, *et al*. Chip-scale droop-free fin light-emitting diodes using facet-selective contacts [J]. *ACS Appl. Mater. Interfaces*, 2021, 13(37): 44663-44672.

[2] NIKOOBAKHT B, HANSEN R P, ZONG Y Q, *et al*. High-brightness lasing at submicrometer enabled by droop-free fin light-emitting diodes (LEDs) [J]. *Sci. Adv.*, 2020, 6(33): eaba4346.

[3] ZHANG Y Y, ZHANG X H, LI K H, *et al*. Advances in Ⅲ-nitride semiconductor microdisk lasers [J]. *Phys. Status Solidi* (A), 2015, 212(5): 960-973.

[4] CHANG S, REX N B, CHANG R K, *et al*. Erratum: "Stimulated emission and lasing in whispering gallery modes of GaN microdisk cavities" [J]. *Appl. Phys. Lett.*, 1999, 75(23): 3719.

[5] ZHANG C J, TU Q M, FRANCIS L F, *et al*. Band gap tuning of films of undoped zno nanocrystals by removal of surface groups [J]. *Nanomaterials*, 2022, 12(3): 565.

[6] ENNACERI H, TALEB A, BOUJNAH M, *et al*. Theoretical and experimental studies of Al-doped ZnO thin films: optical and structural properties [J]. *J. Comput. Electron.*, 2021, 20(5): 1948-1958.

[7] DU J, TANG J H, XU S D, *et al*. ZnO nanoparticles: recent advances in ecotoxicity and risk assessment [J]. *Drug Chem. Toxicol*, 2020, 43(3): 322-333.

[8] BAGNALL D M, CHEN Y F, ZHU Z, *et al*. Optically pumped lasing of ZnO at room temperature [J]. *Appl. Phys. Lett.*, 1997, 70(17): 2230-2232.

[9] CHU S, WANG G P, ZHOU W H, *et al*. Electrically pumped waveguide lasing from ZnO nanowires [J]. *Nat. Nanotechnol.*, 2011, 6(8): 506-510.

[10] XU C X, DAI J, ZHU G P, *et al*. Whispering-gallery mode lasing in ZnO microcavities [J]. *Laser Photonics Rev.*, 2014, 8(4): 469-494.

[11] ZOU B S, LIU R B, WANG F F, *et al*. Lasing mechanism of ZnO nanowires/nanobelts at room temperature [J]. *J. Phys. Chem.* B, 2006, 110(26): 12865-12873.

[12] DAI T F, HSU W C, HSU H C. Improvement of photoluminescence and lasing properties in ZnO submicron spheres by elimination of surface-trapped state [J]. *Opt. Express*, 2014, 22(22): 27169-27174.

[13] DONG H X, ZHOU B E, LI J Z, *et al*. Ultraviolet lasing behavior in ZnO optical microcavities [J]. *J. Mater.*, 2017, 3(4): 255-266.

[14] MIAO C Z, XU H Y, JIANG M M, *et al*. Employing rhodium tripod stars for ultraviolet plasmon enhanced Fabry-Perot mode lasing [J]. *CrystEngComm*, 2020, 22(34): 5578-5586.

[15] LIU X, FANG W, HUANG Y, *et al*. Optically pumped ultraviolet microdisk laser on a silicon substrate [J]. *Appl. Phys. Lett.*, 2004, 84(14): 2488-2490.

[16] RUTH M, ZENTGRAF T, MEIER C. Blue-green emitting microdisks using low-temperature-grown ZnO on patterned silicon substrates [J]. *Opt. Express*, 2013, 21(21): 25517-25525.

[17] SOREF R, DE LEONARDIS F, Classical and quantum photonic sources based upon a nonlinear GaP/Si-superlattice micro-ring resonator [J]. *Chip*, 2022, 1(2): 100011.

[18] QIN F F, SUN Y, YANG Y, *et al*. Optically pumped wavelength-tunable lasing from a GaN beam cavity with an integrated Joule heater pivoted on Si [J]. *Chin. Phys.* B, 2023, 32(5): 054210.

[19] 朱刚毅, 宁波, 仇国庆, 等. InGaN/GaN量子阱悬空微盘发光二极管[J]. 光子学报, 2024, 53(5): 0553116.
ZHU G Y, NING B, QIU G Q, *et al.* InGaN/GaN quantum well led based on floating microdisk cavity [J]. *Acta Photon. Sinica*, 2024, 53(5): 0553116. (in Chinese)

[20] WANG X D, ZHU Y F, JIN T T, *et al.* Waveguide-coupled deterministic quantum light sources and post-growth engineering methods for integrated quantum photonics [J]. *Chip*, 2022, 1(3): 100018.

[21] ARMANI D K, KIPPENBERG T J, SPILLANE S M, *et al.* Ultra-high-*Q* toroid microcavity on a chip [J]. *Nature*, 2003, 421(6926): 925-928.

[22] WANG X X, HUANG C Y, XIA C S, *et al.* Doped microspheres for whispering gallery mode microlasing [J]. *Sci. Bull.*, 2024, 69(13): 2021-2024.

[23] YANG D K, WANG D, HUANG Q S, *et al.* The development of laser-produced plasma EUV light source [J]. *Chip*, 2022, 1(3): 100019.

[24] 秦飞飞, 卢雪瑶, 王潇璇, 等. 硅基InGaN/GaN多量子阱微盘器件的发光、探测和数据传输[J]. 发光学报, 2024, 45(6): 978-985.
QIN F F, LU X Y, WANG X X, *et al.* Light emission, detection and data transmission in silicon-based InGaN/GaN multi-quantum well microdisk device [J]. *Chin. J. Lumin.*, 2024, 45(6): 978-985. (in Chinese)

[25] HAO F, NORDLANDER P. Efficient dielectric function for FDTD simulation of the optical properties of silver and gold nanoparticles [J]. *Chem. Phys. Lett.*, 2007, 446(1-3): 115-118.

[26] ZHANG C F, ZHANG F, SUN X W, *et al.* Frequency-upconverted whispering-gallery-mode lasing in ZnO hexagonal nanodisks [J]. *Opt. Lett.*, 2009, 34(21): 3349-3351.

[27] 朱刚毅, 仇国庆, 秦飞飞, 等. 悬空车轮形氮化镓发光二极管[J]. 发光学报, 2020, 41(9): 1146-1152.
ZHU G Y, QIU G Q, QIN F F, *et al.* Floating GaN micro wheel light emitting diodes [J]. *Chin. J. Lumin.*, 2020, 41(9): 1146-1152. (in Chinese)

[28] QIN F F, XU C X, ZHU Q X, *et al.* Optical performance improvement in hydrothermal ZnO/graphene structures for ultraviolet lasing [J]. *J. Mater. Chem.* C, 2018, 6(13): 3240-3244.

[29] FONOBEROV V A, BALANDIN A A, Origin of ultraviolet photoluminescence in ZnO quantum dots: confined excitons versus surface-bound impurity exciton complexes [J]. *Appl. Phys. Lett.*, 2004, 85(24): 5971-5973.

[30] XIU F X, YANG Z, ZHAO D T, *et al.* ZnO growth on Si with low-temperature ZnO buffer layers by ECR-assisted MBE [J]. *J. Cryst. Growth*, 2006, 286(1): 61-65.

[31] PEI Z X, DING L Y, LU M L, *et al.* Synergistic effect in polyaniline-hybrid defective ZnO with enhanced photocatalytic activity and stability [J]. *J. Phys. Chem.* C, 2014, 118(18): 9570-9577.

[32] KOTSIS K, STAEMMLER V. *Ab initio* calculations of the O1s XPS spectra of ZnO and Zn oxo compounds [J]. *Phys. Chem. Chem. Phys.*, 2006, 8(13): 1490-1498.

[33] REYNOLDS D C, LOOK D C, JOGAI B, *et al.* Time-resolved photoluminescence lifetime measurements of the Γ_5 and Γ_6 free excitons in ZnO [J]. *J. Appl. Phys.*, 2000, 88(4): 2152-2153.

[34] KOIDA T, CHICHIBU S F, UEDONO A, *et al.* Correlation between the photoluminescence lifetime and defect density in bulk and epitaxial ZnO [J]. *Appl. Phys. Lett.*, 2003, 82(4): 532-534.

[35] 郭士亮, 胡春海, 李欣, 等. 一种新型高灵敏度光学微环湿度传感器[J]. 发光学报, 2014, 35(8): 1009-1013.
GUO S L, HU C H, LI X, *et al.* A novel high sensitivity optical microresonator humidity sensor [J]. *Chin. J. Lumin.*, 2014, 35(8): 1009-1013. (in Chinese)

[36] 李文媛, 付鑫鹏, 姚聪, 等. 基于回音壁模式光学微腔的低阈值激光器研究进展[J]. 发光学报, 2022, 43(12): 1823-1838.
LI W Y, FU X P, YAO C, *et al.* Research progress of low threshold laser based on whispering gallery mode microcavity [J]. *Chin. J. Lumin.*, 2022, 43(12): 1823-1838. (in Chinese)

[37] ZHU G Y, TIAN M F, ALMOKHTAR M, *et al.* Whispering gallery mode lasing performance's evolution of floating gan microdisks varying with their thickness [J]. *Chin. Phys. Lett.*, 2022, 39(12): 123401.

[38] JOHNSON J C, YAN H Q, YANG P D, *et al.* Optical cavity effects in ZnO nanowire lasers and waveguides [J]. *Phys. Chem.* B, 2003, 107(34): 8816-8828.

[39] FALLERT J, DIETZ R J B, SARTOR J, *et al.* Co-existence of strongly and weakly localized random laser modes [J].

Nat. Photonics, 2009, 3(5): 279-282.

[40] MUTH J F, KOLBAS R M, SHARMA A K, *et al*. Excitonic structure and absorption coefficient measurements of ZnO single crystal epitaxial films deposited by pulsed laser deposition [J]. *J. Appl. Phys.*, 1999, 85(11): 7884-7887.

[41] GHOSH S, SAHA M, DE S K. Tunable surface plasmon resonance and enhanced electrical conductivity of In doped ZnO colloidal nanocrystals [J]. *Nanoscale*, 2014, 6(12): 7039-7051.

[42] LU J G, FUJITA S, KAWAHARAMURA T, *et al*. Carrier concentration dependence of band gap shift in *n*-type ZnO∶Al films [J]. *J. Appl. Phys.*, 2007, 101(8): 083705.

[43] CHEN L Z, ZHAO J, YANG X F. Regularized linear schemes for the molecular beam epitaxy model with slope selection [J]. *Appl. Numer. Math.*, 2018, 128: 139-156.

[44] NISHIKUBO R, ISHIDA N, KATSUKI Y, *et al*. Minute-scale degradation and shift of valence-band maxima of $(CH_3NH_3)SnI_3$ and $HC(NH_2)_2SnI_3$ perovskites upon air exposure [J]. *J. Phys. Chem.* C, 2017, 121(6): 19650-19656.

[45] ZHANG H J, BERTHOD C, BERGER H, *et al*. Band filling and cross quantum capacitance in ion-gated semiconducting transition metal dichalcogenide monolayers [J]. *Nano Lett.*, 2019, 19(12): 8836-8845.

[46] DJURIŠIĆ A B, LEUNG Y H. Optical properties of ZnO nanostructures [J]. *Small*, 2006, 2(8-9): 944-961.

朱刚毅(1980-),男,河南洛阳人,博士,副教授,硕士生导师,2013年于东南大学获得博士学位,主要从事宽禁带半导体微腔光电特性的研究。

E-mail: zhugangyi@njupt. edu. cn